Biochimica et Biophysica Acta 1828 (2013) 1926–1937

Contents lists available at SciVerse ScienceDirect

Biochimica et Biophysica Acta

journal homepage: www.elsevier.com/locate/bbamem

Deciphering the role of charge, hydration, and hydrophobicity for cytotoxic activities and membrane interactions of bile acid based facial amphiphiles

Manish Singh [1], Ashima Singh [1], Somanath Kundu [1], Sandhya Bansal, Avinash Bajaj *

The Laboratory of Nanotechnology and Chemical Biology, Regional Centre for Biotechnology, 180 Udyog Vihar, Phase 1, Gurgaon-122016, Haryana, India

ARTICLE INFO

Article history:
Received 24 January 2013
Received in revised form 21 March 2013
Accepted 8 April 2013
Available online 13 April 2013

Keywords:
Facial amphiphiles
Bile acids
Cytotoxicity
Model membranes
Cancer

ABSTRACT

We synthesized four cationic bile acid based facial amphiphiles featuring trimethyl ammonium head groups. We evaluated the role of these amphiphiles for cytotoxic activities against colon cancer cells and their membrane interactions by varying charge, hydration and hydrophobicity. The singly charged cationic Lithocholic acid based amphiphile (**LCA-TMA$_1$**) is most cytotoxic, whereas the triply charged cationic Cholic acid based amphiphile (**CA-TMA$_3$**) is least cytotoxic. Light microscopy and Annexin-FITC assay revealed that these facial amphiphiles caused late apoptosis. In addition, we studied the interactions of these amphiphiles with model membrane systems by Prodan-based hydration, DPH-based anisotropy, and differential scanning calorimetry. **LCA-TMA$_1$** is most hydrophobic with a hard charge causing efficient dehydration and maximum perturbations of membranes thereby facilitating translocation and high cytotoxicity against colon cancer cells. In contrast, the highly hydrated and multiple charged **CA-TMA$_3$** caused least membrane perturbations leading to low translocation and less cytotoxicity. As expected, Chenodeoxycholic acid and Deoxycholic acid based amphiphiles (**CDCA-TMA$_2$**, **DCA-TMA$_2$**) featuring two charged head groups showed intermediate behavior. Thus, we deciphered that charge, hydration, and hydrophobicity of these amphiphiles govern membrane interactions, translocation, and resulting cytoxicity against colon cancer cells.

1. Introduction

Bile acids are naturally occurring steroids produced from metabolism of cholesterol in liver, and promote solubilization and absorption of fats, nutrients, and vitamins in intestine [1]. Bile acids are facial amphiphiles in which hydrophobic and hydrophilic parts are located on opposite faces, as compared to surfactants [2]. This unique structural aspect of bile acids contributes towards the overall amphiphilic molecular architecture leading to variety of functions including membrane interactions and cytotoxicity. For example, the hydrophobicity of bile acids is inversely related to the number of polar OH groups. The increase in hydrophobicity of bile acids confers toxicity [3]. In humans, cholic acid (CA) and chenodeoxycholic acid (CDCA) are primary bile acids, whereas deoxycholic acid (DCA) and lithocholic acid (LCA) are secondary bile acids. Primary bile acids upon conjugation with glycine or taurine become less hydrophobic and show less toxicity [4], whereas secondary bile acids are more hydrophobic and thus feature more cytotoxicity. Population based studies indicate that consumption of Western diet increases levels of fecal secondary bile acids [5]. This excessive deposition of bile acids is responsible for oxidative DNA damage, inflammation, and enhanced cellular proliferation against colon epithelial cells leading to colon cancer [6].

Anticancer activities of bile acids can be attributed either to their nonspecific detergent effects or specific receptor-mediated interactions [7]. Bile acids can trigger apoptosis by altering physical characteristics of cell membranes through non-specific interactions [8]. Bile acids can also specifically bind to receptors leading to cellular toxicity [9,10]. Different mechanisms [11] of bile acids induced apoptosis [12] have been proposed including endoplasmic reticulum stress, ligand-independent activation of death receptor pathways, and mitochondrial intrinsic pathway [13]. Both natural and synthetic bile acids show diverse bioactivities including both apoptotic and cell-proliferative behavior contingent upon the nature of their molecular architectures [14,15]. To this end, numerous bile acid derivatives have been synthesized [16,17] and evaluated for their anticancer activities against array of cancer cell lines [18].

We hypothesized that the introduction of cationic charge to bile acids would favor the electrostatic interactions of these amphiphiles with cell membranes and therefore can improve their cytotoxic effect. Towards this goal, we synthesized four bile acid based facial cationic amphiphiles to evaluate their cytotoxicity against colon cancer cells and membrane interactions. Trimethylamonium group was conjugated to hydroxyl group of LCA, CDCA, DCA, and CA (Fig. 1). We studied the cytotoxic activities of these facial amphiphiles in two colon cancer cell lines (HCT-116, DLD-1) using MTT assay, and evaluated the mechanism of cytotoxicity by light microscopy and apoptosis assay. We then studied interactions

* Corresponding author. Tel.: +91 124 2848831; fax: +91 124 4038117.
E-mail address: bajaj@rcb.res.in (A. Bajaj).
[1] These Authors contributed equally.

0005-2736/$ – see front matter © 2013 Elsevier B.V. All rights reserved.
http://dx.doi.org/10.1016/j.bbamem.2013.04.003

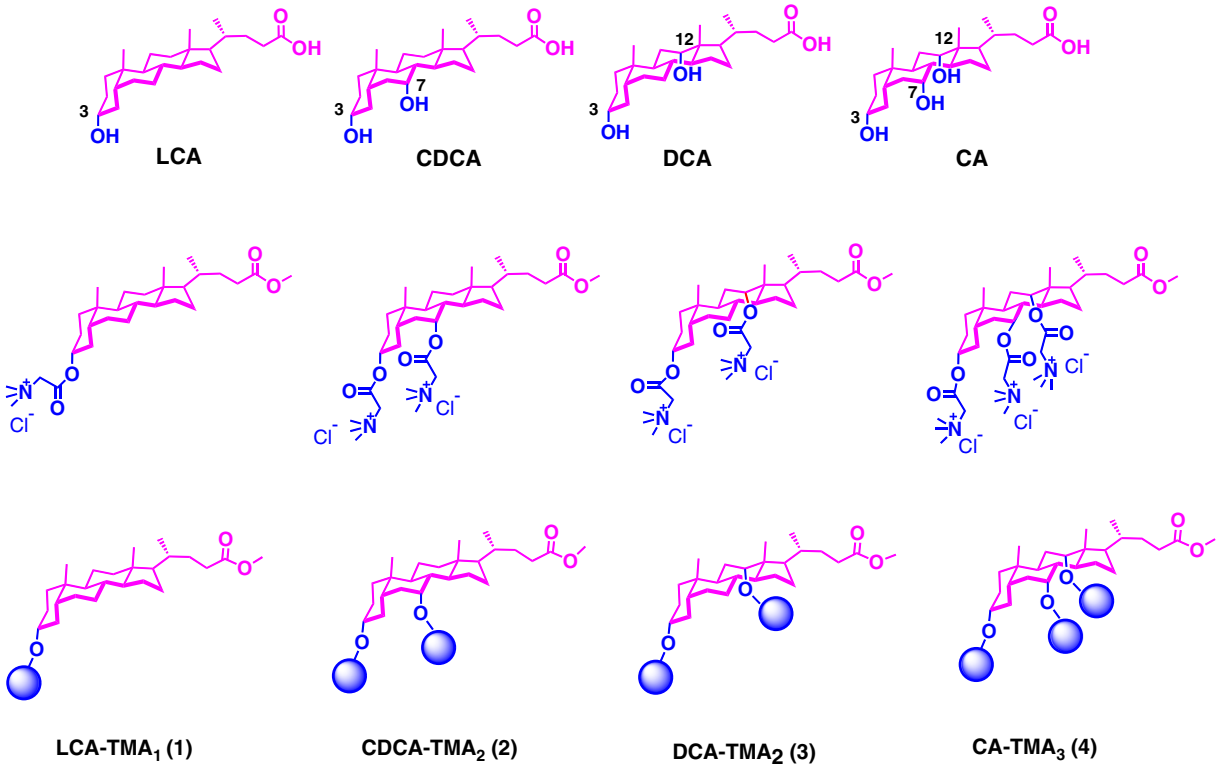

Fig. 1. Molecular structures of the bile acids: lithocholic acid (LCA), chenodeoxycholic acid (CDCA), deoxycholic acid (DCA), and cholic acid (CA); and corresponding synthesized facial amphiphiles LCA-TMA_1, CDCA-TMA_2, DCA-TMA_2, and CA-TMA_3 studied.

of these amphiphiles with model DPPC membranes using Prodan-based hydration, DPH-based anisotropy, and differential scanning calorimetry to evaluate their differential cytotoxic activities by varying charge, hydration, and hydrophobicity.

2. Materials and methods

2.1. General

All the chemicals, reagents, and solvents used are of highest purity available. ^{1}H-NMR spectra were recorded using Bruker 500 MHz spectrometer. Chemical shifts (δ) are reported in ppm with tetramethyl silane as internal standard. Mass spectras were measured on AB-SCIEX-5600 mass spectrometer.

2.2. General procedure for synthesis of bile acid methyl esters (9–12)

Bile acids (5–8) (2.65 mmol) were dissolved in anhydrous methanol (40 mL), and conc. hydrochloric acid (1 mL) was added. Reaction mixture was stirred for 12 h at room temperature. After completion of reaction, solvent was evaporated under vacuum and reaction mixture was diluted with ethyl acetate (50 mL). Reaction mixture was washed with sodium bicarbonate (2 × 10 mL) and brine (2 × 5 mL). Organic phase was dried over sodium sulfate and concentrated in vacuum to obtain pure product.

2.2.1. Methyl 3α-hydroxy-5β-lithocholan-24-oate (9)

Yield 94%. ^{1}H NMR ($CDCl_3$, 500 MHz) δ: 0.62 (*s*, 3H), 0.74–2.30 (*m*), 3.45 (*m*, 1H), 3.56 (*s*, 3H). HRMS (ESI) : m/z $(C_{25}H_{42}O_3)^+$ calculated $(M + H_2O)^+$ 408.3240; found $(M + H_2O)^+$ 408.3522, calculated $(M + Na)^+$ 413.3032; found $(M + Na)^+$ 413.3076.

2.2.2. Methyl 3α, 7α-dihydroxy-5β-chenodeoxycholan-24-oate (10)

Yield 92%. ^{1}H NMR ($CDCl_3$, 500 MHz) δ: 0.67 (*s*, 3H), 0.90–2.34 (*m*), 3.58–3.64 (*m*, 1H), 3.66 (*s*, 3H), 3.97 (*m*, 1H). HRMS (ESI): m/z $(C_{25}H_{42}O_4)^+$ calculated $(M + H)^+$ 407.3083; found $(M + H)^+$ 407.3231, calculated $(M + H_2O)^+$; 424.3189, found $(M + H_2O)^+$ 424.3485, calculated $(M + Na)^+$ 429.2981; found $(M + Na)^+$ 429.3062.

2.2.3. Methyl 3α, 7α, 12α-dihydroxy-5β-deoxycholan-24-oate (11)

Yield 90%. ^{1}H NMR ($CDCl_3$, 500 MHz) δ: 0.62 (*s*, 3H), 0.89–2.34 (*m*), 3.40–3.51 (*m*, 1H), 3.65 (*s*, 3H), 3.84 (*m*, 1H)). HRMS (ESI): m/z $(C_{25}H_{42}O_4)^+$ calculated $(M + H)^+$ 407.3083; found $(M + H)^+$ 407.3202, calculated $(M + H_2O)^+$ 424.3189; found $(M + H_2O)^+$ 424.3485, calculated $(M + Na)^+$ 429.2981; found $(M + Na)^+$ 429.3033.

2.2.4. Methyl-3α, 7α, 12α-trihydroxy-5β-cholan-24-oate (12)

Yield 92%. ^{1}H NMR ($CDCl_3$, 500 MHz) δ: 0.67 (*s*, 3H), 0.86–2.37 (*m*), 3.40–3.46 (*m*, 1H), 3.66 (*s*, 3H), 3.84 (*m*, 1H), 3.96 (*m*, 1H). HRMS (ESI) : m/z $(C_{25}H_{42}O_5)^+$ calculated $(M + H)^+$ 423.3032; found $(M + H)^+$ 423.3169, calculated $(M + H_2O)^+$ 440.3138; found $(M + H_2O)^+$ 440.3440, calculated $(M + Na)^+$ 445.2930, found $(M + Na)^+$ 445.2987.

2.3. General procedure for synthesis of (2′-chloroacetoxy) derivative of bile acid methyl esters (13–16)

To a solution of 9–12 (1.28 mmol) in toluene (20 mL), DMAP (0.38 mmol), pyridine (1 mL) and chloroacetic anhydride (1.2 equiv for 9; 2.4 equiv for 10 & 11; 3.6 equiv for 12) was added. Reaction mixture was heated at 60 °C for 48 h. Solvent was evaporated and diluted with ethyl acetate (50 mL). Reaction mixture was washed with brine solution

(2 × 10 mL). Crude product was purified by chromatography using ethyl acetate: pet ether as eluent to obtain pure compound.

2.3.1. Methyl 3α-chloroacetyloxy-5β-lithocholan-24-oate (13)

Yield 68%. ^{1}H NMR ($CDCl_3$, 500 MHz) δ: 0.67 (*s*, 3H), 0.93–2.10 (*m*), 3.69 (*s*, 3H), 4.05 (*s*, 2H), 4.84 (*m*, 1H). HRMS (ESI): m/z $(C_{27}H_{43}ClO_4)^+$ calculated $(M + Na)^+$ 489.2748; found $(M + Na)^+$ 489.2795.

2.3.2. Methyl 3α, 7α-bis (chloroacetyloxy)-5β-chenodeoxycholan-24-oate (14)

Yield 63%. ^{1}H NMR ($CDCl_3$, 500 MHz) δ: 0.64 (*s*, 3H), 0.87–2.35 (*m*), 3.73 (*s*, 3H), 3.97–4.02 (*m*, 4H), 4.65–4.70 (*m*, 1H), 4.99 (*m*, 1H). HRMS (ESI): m/z $(C_{29}H_{44}Cl_2O_6^+)$ calculated $(M + Na)^+$ 581.2413; found $(M + Na)^+$ 581.2734, calculated $(M + H_2O)^+$ 576.2621; found $(M + H_2O)^+$ 576.3180.

2.3.3. Methyl 3α, 12α-bis (chloroacetyloxy)-5β-deoxycholan-24-oate (15)

Yield 66%. ^{1}H NMR ($CDCl_3$, 500 MHz) δ: 0.74 (*s*, 3H), 0.80–2.34 (*m*), 3.80 (*s*, 3H), 4.03 (*s*, 2H), 4.11 (*s*, 2H), 4.77–4.81 (*m*, 1H), 5.00–5.41 (*m*, 1H). HRMS (ESI) : m/z $(C_{29}H_{44}Cl_2O_6)^+$ calculated $(M + Na)^+$ 581.2413; found $(M + Na)^+$ 581.2413, calculated $(M + H_2O)^+$ 576.2621; found $(M + H_2O)^+$ 576.2947.

2.3.4. Methyl 3α, 7α, 12α-Tris (chloroacetyloxy)-5β-cholan-24-oate (16)

Yield 67%. ^{1}H NMR ($CDCl_3$, 500 MHz) δ: 0.75 (*s*, 3H), 0.81–2.33 (*m*), 3.48 (*s*, 3H), 3.80–3.97 (*m*, 6H), 4.62–4.71 (*m*, 1H), 5.03–5.19 (*m*, 1H), 5.29–5.34 (*m*, 1H). HRMS (ESI): m/z $(C_{31}H_{45}Cl_3O_8)^+$ calculated $(M + Na)^+$ 673.2078; found $(M + Na)^+$ 673.2069, calculated $(M + H_2O)^+$ 668.2286; found $(M + H_2O)^+$ 668.2564.

2.4. General procedure for the synthesis of mono, di and tricationic lipids (1–4)

Compound 13–16 (0.21 mmol) was dissolved in ethyl acetate (5 mL) in seal tube. Trimethyl amine gas was added into it. Reaction mixture was heated at 70 °C for 48 h. After completion of reaction, solvent was removed. Reaction mixture was washed with ethyl acetate and acetone multiple times to furnish pure compound.

2.4.1. LCA-TMA$_1$ (1)

Yield 72%. ^{1}H NMR ($CDCl_3$, 500 MHz) δ: 0.58 (*s*, 3H), 0.84–2.29 (*m*), 3.54–3.61(*m*, 12H), 4.7 (*m*, 1H), 5.01 (*m*, 2H). HRMS (ESI) : m/z $(C_{30}H_{52}NO_4)^+$ calculated $(M)^+$ 490.3896; found $(M)^+$ 490.3897.

2.4.2. CDCA-TMA$_2$ (2)

Yield 65%. ^{1}H NMR ($CDCl_3$, 500 MHz) δ: 0.64 (*s*, 3H), 0.82–2.36 (*m*), 3.10–3.65 (*m*, 21H), 3.87–3.95 (*m*, 1H), 4.07–4.11 (*m*, 1H), 4.52–4.60 (*m*, 1H), 4.75–4.78 (*m*, 1H), 5.02–5.07 (*m*, 1H), 5.48–5.54 (*m*, 1H). HRMS (ESI): m/z $(C_{35}H_{62}N_2O_6)^{+2}/2$ calculated 303.2303; found $(M)^{+2}/2$ 303.2308, $M^{2+}Cl^-$ calculated 641.4296; found $M^{2+}Cl^-$ 641.4279.

2.4.3. DCA-TMA$_2$ (3)

Yield 68%. ^{1}H NMR ($CDCl_3$, 500 MHz) δ: 0.73 (*s*, 3H), 0.79–2.32 (*m*), 3.54–3.68 (*m*, 21H), 4.08–4.13 (*m*, 1H), 4.76–4.80 (*m*, 1H), 5.06 (*d*, 1H). 5.29 (*d*, 1H), 5.47 (*d*, 1H), 5.55 (*d*, 1H). HRMS (ESI): m/z $(C_{35}H_{62}N_2O_6)^{+2}/2$ calculated 303.2303; found $(M)^{+2}/2$ 303.2308, $M^{2+}Cl^-$ calculated 641.4296; found $M^{2+}Cl^-$ 641.4279.

2.4.4. CA-TMA$_3$ (4)

Yield 71%. ^{1}H NMR ($CDCl_3$, 500 MHz) δ: 0.75 (*s*, 3H), 0.82–2.40 (*m*), 3.53–3.62 (*m*, 30H), 3.74 (*m*, 2H), 4.09 (*m*, 1H), 4.78 (*m*, 1H), 5.11 (*m*, 2H), 5.29 (*m*, 2H), 5.80 (*m*, 1H). HRMS (ESI): m/z $(C_{40}H_{72}N_3O_8)^{+3}/3$ calculated 240.8439; found $(M)^{+3}/3$ 240.8429, $M^{3+}Cl^-/2$ calculated 378.7504; found $M^{3+}Cl^-/2$ 378.7507, $M^{3+}Cl^{2-}$ calculated 792.4696; found $M^{3+}Cl^{2-}$ 792.4687.

2.5. Cell culture

Colon cancer cells HCT-116 and DLD-1 were maintained as monolayers for experiments. HCT-116 cells were cultured in McCoy's 5A media, and DLD-1 cells were cultured in RPMI-1640 (Cell clone, USA) media containing 10% (v/v) fetal bovine serum, penicillin 100 μg/mL, streptomycin 100 U/mL, gentamycin 45 μg/mL at 37 °C in a humidified atmosphere with 5% CO_2.

2.6. Cell viability assay

Cell viability for all amphiphiles in two different colon cancer cell lines was measured using 3-[4, 5-dimethylthiazol-2-yl] 2, 5-diphenyltetrazolium bromide (MTT) assay [19]. HCT-116 or DLD-1 were plated in 96 well tissue culture plate at a density of 3000 cells per well. After 24 h, cells were treated with various bile acids and facial amphiphiles at concentrations of 25, 50, 100, 150 and 200 μM. After 48 h of treatment, 20 μL of MTT solution (5 mg/mL) was added to each well and further incubated for 3 h to get formazan crystals. Media was aspirated and 150 μL of DMSO was added to lyse cells. Plate was shaken for 10 min and absorbance was recorded at 540 nm using spectramax M5 (Molecular devices). Cell viability was then calculated using equation [{A_{540} (treated cells) − background] / [A_{540} (untreated cells) − background}] 100, and graphs were plotted using Graph pad Prism 5 software.

2.7. Light microscopy and Annexin V-FITC assay

Annexin V-FITC assay was performed in order to find out percentage of apoptotic cells [20]. HCT-116 or DLD-1 cells (2×10^5 cells/ well) were seeded onto each well in 6 well plates for 24 h for adherence. Cells were treated with 50 μM of bile acid based facial amphiphiles for HCT-116 cells and with 100 μM for DLD-1 cells. Cells were visualized under light microscope before processing for Annexin-FITC assay. After 48 h of treatment, cells were trypsinized and collected by centrifugation for 5 minutes at 2,000 rpm. Cells were re-suspended at a density of 1×10^6 cells/mL in binding buffer (as provided with kit). Cells were then stained simultaneously with FITC labeled Annexin V (50 μg/mL) and propidium iodide (100 μg/mL). Cells were analyzed using a flow cytometer (Becton Dickinson) and data was analyzed with FACSuite software.

2.8. Liposome formation [21]

Thin films of DPPC lipids were prepared under dry argon gas by taking desired amount of DPPC in chloroform in round-bottom Wheaton glass. Thin films were dried under vacuum for 6 h and were hydrated with Milli Q water for at least 12 h. Multilamellar vesicles were prepared using hydrated films by 4–5 freeze thaw cycles from 70 °C to 4 °C with intermittent vortexing. Unilamellar vesicles were prepared by sonication of samples at 70 °C for 15 min.

2.9. Prodan based hydration studies

DPPC liposomes doped with Prodan [22] as a probe were prepared as described above. We studied changes in surface hydration of DPPC membranes on incubation of Prodan doped DPPC liposomes with 10, 20, and 30 mole percentages of facial amphiphiles at 37 °C to mimic *in vitro* cell culture conditions. We recorded generalized polarization of Prodan at times points of 6 h, 12 h, 24 h, and 48 h in 96-well plate in Molecular Devices M5 instrument. Fluorescence of Prodan was recorded using λ_{ex} of 350 nm and end point emissions at λ_{em} of 440 nm and 490 nm. Generalized polarization (GP) was calculated using equation $GP = (I_{440} - I_{490}) / (I_{440} + I_{490})$.

2.10. Fluorescence anisotropy studies

DPPC liposomes were prepared using DPH probe by freeze-thaw cycles as described earlier [23]. DPH doped DPPC vesicles were incubated with 10, 20, and 30 mole percentages of facial amphiphiles at 37 °C. We measured changes in steady state anisotropy of DPH at 37 °C at different time intervals (6 h, 12 h, 24 h, 48 h) in 96-well plate using fluorescence anisotropy protocol in Molecular devices M5 instrument with λ_{ex} at 350 nm and λ_{em} of 452 nm.

2.11. Differential scanning calorimetry [24]

DPPC liposomes were incubated with 10, 20, and 30 mole percentages of facial amphiphiles at 37 °C for 24 h. After 24 h of incubation, these DPPC liposomes-amphiphile mixtures were studied by differential scanning calorimetry studies using Nano DSC instrument, TA instruments, USA. Degassing was performed on all reference and sample solutions to minimize possibility of gas bubble formation during run. We performed all experiments by measuring DSC thermograms in temperature range of 20–60 °C with heating and cooling scan rates at 1.0 °C/min. Data analysis was performed by subtracting respective baseline thermogram from sample thermogram using NanoAnalyze software. DSC thermograms were plotted from "excess heat capacity" and temperature. We calculated maxima point of excess heat capacity (C_p^{max}), calorimetric enthalpies (ΔH_c), entropies (ΔS) and full width at half maxima (FWHM). T_m is absolute phase transition temperature of sample. C_p^{max} is maxima point of excess heat capacity in main transition peak. Maximum of C_p vs. T curve is C_p^{max}. The van't Hoff enthalpy is expressed by [25]

$$\Delta H_{vH} = \left(4RT_m{}^2 C_p{}^{max}\right)/(\Delta H_c) \approx \left(6.9T_m{}^2/\Delta T_{1/2}\right)$$

Size of co-operativity unit (CU) for phase transition was determined using formula [26]

$$CU = \Delta H_{vH}/\Delta H_c$$

We analyzed different domains of multicomponent melting curves using two state scaled hypothesis [27] by NanoAnalyze Software.

3. Results and discussion

3.1. Synthesis and characterization of facial amphiphiles

Bile acid based facial amphiphiles (Fig. 1) were synthesized from corresponding bile acids in three-step procedures (Scheme 1). Briefly, bile acids (5–8) were esterified with MeOH in presence of HCl to obtain corresponding bile acid methyl esters (9–12) in quantitative yields. Methyl esters of bile acids (9–12) were then reacted with chloroacetic anhydride at 60 °C for 48 h to form chloroacetyl derivatives (13–16). Finally, the chloroacetyl derivatives were reacted with trimethyl amine in ethyl

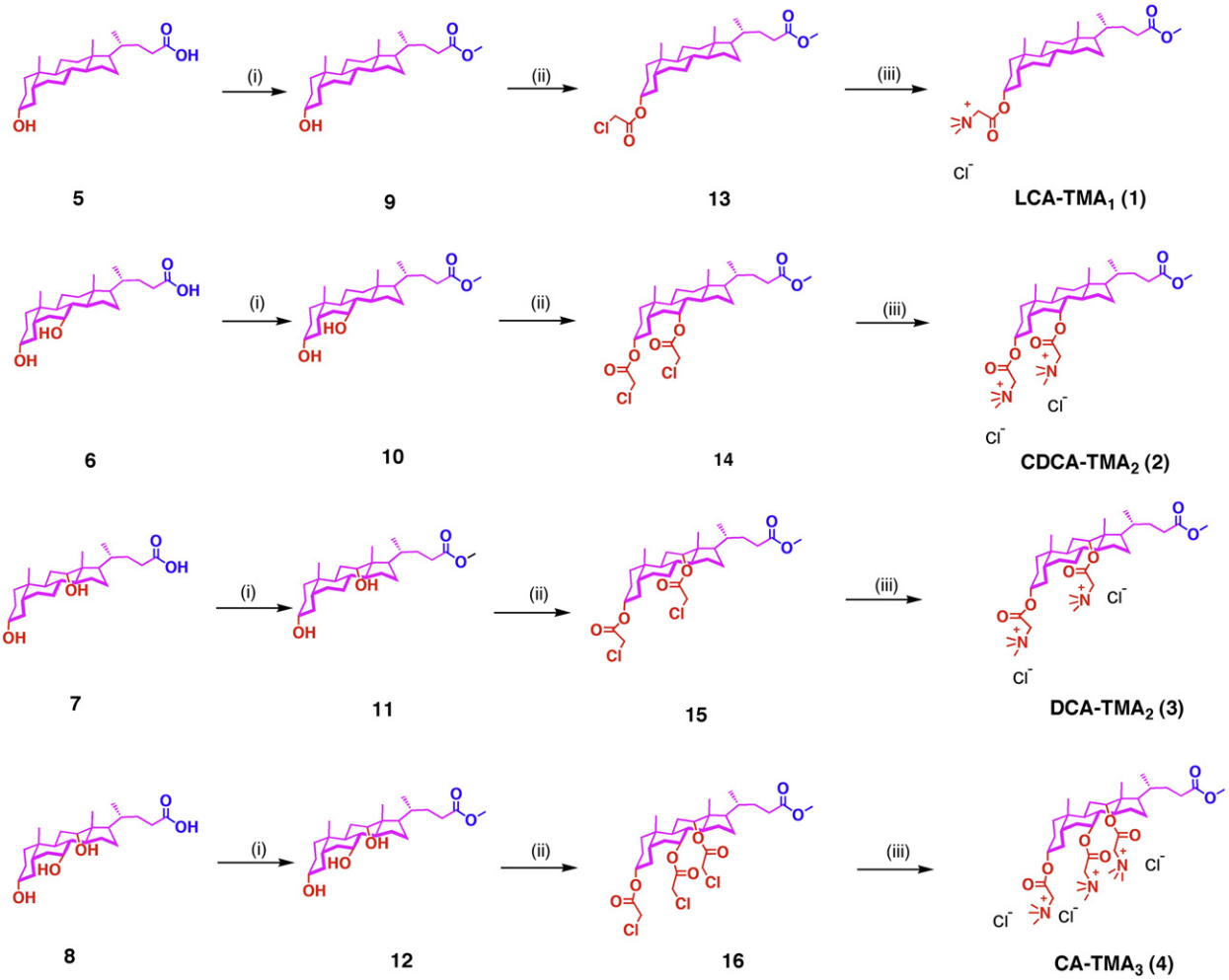

Scheme 1. Reagents, reaction condition, and yields: (i) Methanol, Conc. HCl, rt, 6 h, 90–92% (ii) DMAP, pyridine, chloroaceticanhydride, toluene, 60 °C, 48 h, 63–73% (iii) trimethylamine, ethylacetate, 70 °C, 72 h, 65–72%.

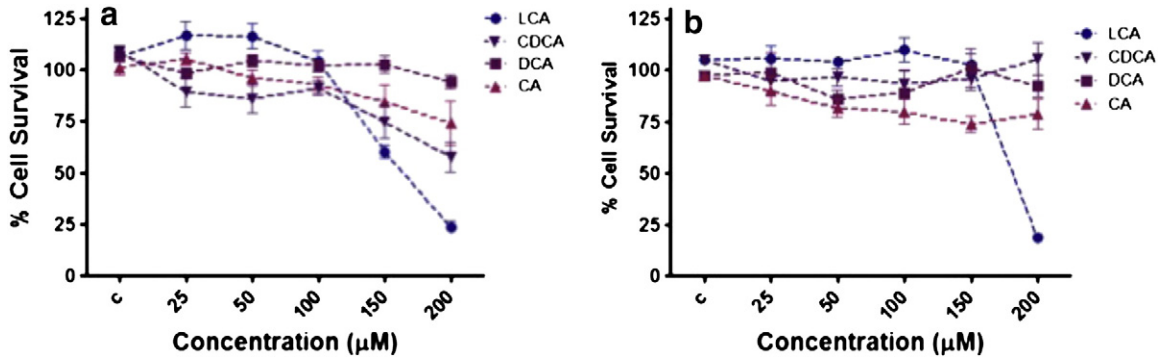

Fig. 2. Anticancer activities of bile acids lithocholic acid (LCA), chenodeoxycholic acid (CDCA), deoxycholic acid (DCA), and cholic acid (CA) in two colon cancer cell lines HCT-116 (a) and DLD-1 (b) upon treatment at 25, 50, 100, 150, 200 mM concentrations for 48 h.

acetate at 70 °C in sealed tube for 48 h to furnish the desired compounds (1–4). Facial amphiphiles were then purified *via* repeated precipitation from ethyl acetate and acetone. The purity and identity of the compounds were confirmed by ^{1}H NMR, and Mass spectroscopy.

3.2. Cytotoxicity of facial amphiphiles

Bile acids (LCA, CDCA, DCA, CA) alone can cause cellular toxicities at conc. of 150 μM and 200 μM in HCT-116 cells (Fig. 2a). At 200 μM, we observed 75%, 40%, and 25% cellular toxicity for LCA, CDCA and CA respectively, whereas DCA was found to be inactive up to 200 μM. Therefore, the order of activities of bile acids in HCT-116 cells is LCA > CDCA > CA > DCA. In DLD-1 cells, CDCA and DCA are not active up to 200 μM, and CA causes 20% toxicity (Fig. 2b) at 200 μM. As in case of HCT-116 cells, most hydrophobic bile acid LCA shows 80% cellular toxicity at 200 μM in DLD-1 cells. Thus, the primary and secondary bile acids show basal level activity against both HCT-116 and DLD-1 cell lines.

To probe the role of charge on cytotoxicity at various concentrations, we evaluated four of these bile acid based facial amphiphiles LCA-TMA_1, CDCA-TMA_2, DCA-TMA_2, CA-TMA_3 against HCT-116 and DLD-1 cell lines (Fig. 3). Treatment of HCT-116 cells with 25 μM LCA-TMA_1 showed 50% cell viability whereas CDCA-TMA_2 and DCA-TMA_2 amphiphiles with two ammonium head groups showed no activity at similar concentration (Fig. 3a). Additionally, upon increasing the concentration of LCA-TMA_1 to 100 μM, we observed 75% cellular toxicity whereas CDCA-TMA_2 and DCA-TMA_2 showed diminished activity of only 25% and 50%, respectively. However, the introduction of multiple charges on Cholic Acid does not make it highly active as CA-TMA_3 amphiphile showed only 15–25% cellular activity in tested concentrations. Thus, the cytotoxicity of facial amphiphiles against HCT-116 cells showed the order of activities as LCA-TMA_1 > DCA-TMA_2 > CDCA-TMA_2 > CA-TMA_3, featuring LCA-TMA_1 the most active facial amphiphile.

To explore generality of this trend, we studied cytotoxicity of these amphiphiles in another colon cancer cell line DLD-1 (Fig. 3b). As expected, LCA-TMA_1 is most potent cytotoxic agent causing 80% cell death at 100 μM in DLD-1 cells, whereas multi-charged CA-TMA_3 did not show any activity at similar concentration (Fig. 3b). Additionally, CDCA-TMA_2 and DCA-TMA_2 showed 50% and 90% activities at 200 μM, respectively. These facial amphiphiles showed toxicities at higher concentrations in DLD-1 cells as compared to HCT-116 cells, might be due to difference in origins of these cell lines but concomitantly keeping the order of cytotoxicity profile unaltered. Thus, the toxicity studies showed that introduction of single charge on hydrophobic bile acid lithocholic acid enhances the toxicity of bile acids, whereas introduction of multiple charges does not improve the toxicity of other bile acids.

3.3. Light microscopy and annexin-FITC studies

To explore the cytotoxicity of bile acid based amphiphiles, we performed the light microscopy and Annexin-FITC based apoptosis assay. Treatment of HCT-116 cells with LCA-TMA_1 at 50 μM showed maximum number of apoptotic bodies, whereas other amphiphiles showed marginal effect (Fig. 4). In case of DLD-1 cells, treatment of CDCA-TMA_2 and CA-TMA_3 amphiphile did not cause any apoptosis; in contrast DCA-TMA_2 triggered apoptosis. DLD-1 cells on incubation with LCA-TMA_1 at 100 μM showed maximum number of apoptotic bodies (Fig. 5). These results showed that these facial amphiphiles can cause apoptosis both in HCT-116 and DLD-1 cells, and LCA-TMA_1 is most effective causing maximum apoptosis as compared to other amphiphiles.

We studied Annexin-FITC based apoptosis assay (Figs. 6, 7) with these bile acid based amphiphiles. LCA-TMA_1 (50 μM) induced 15% of HCT-116

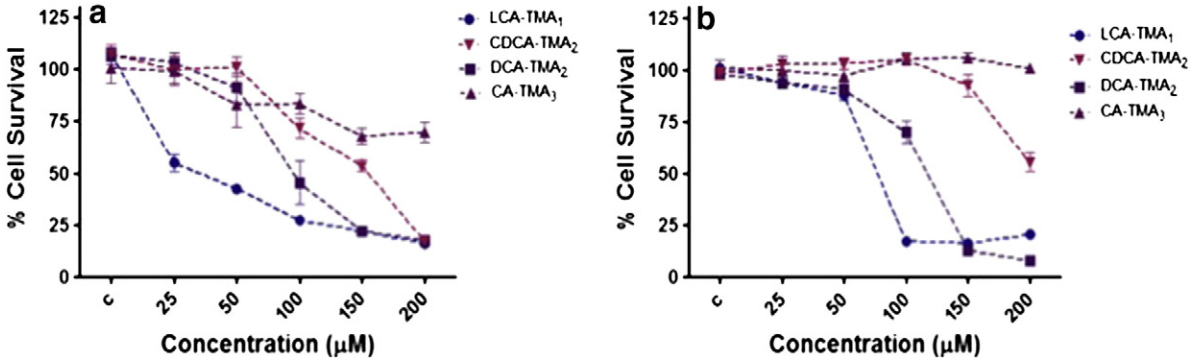

Fig. 3. Anticancer activities of facial amphiphiles LCA-TMA_1, CDCA-TMA_2, DCA-TMA_2, and CA-TMA_3 in two colon cancer cell lines HCT-116 (a) and DLD-1 (b) upon treatment at 25, 50, 100, 150, 200 μM concentrations for 48 h.

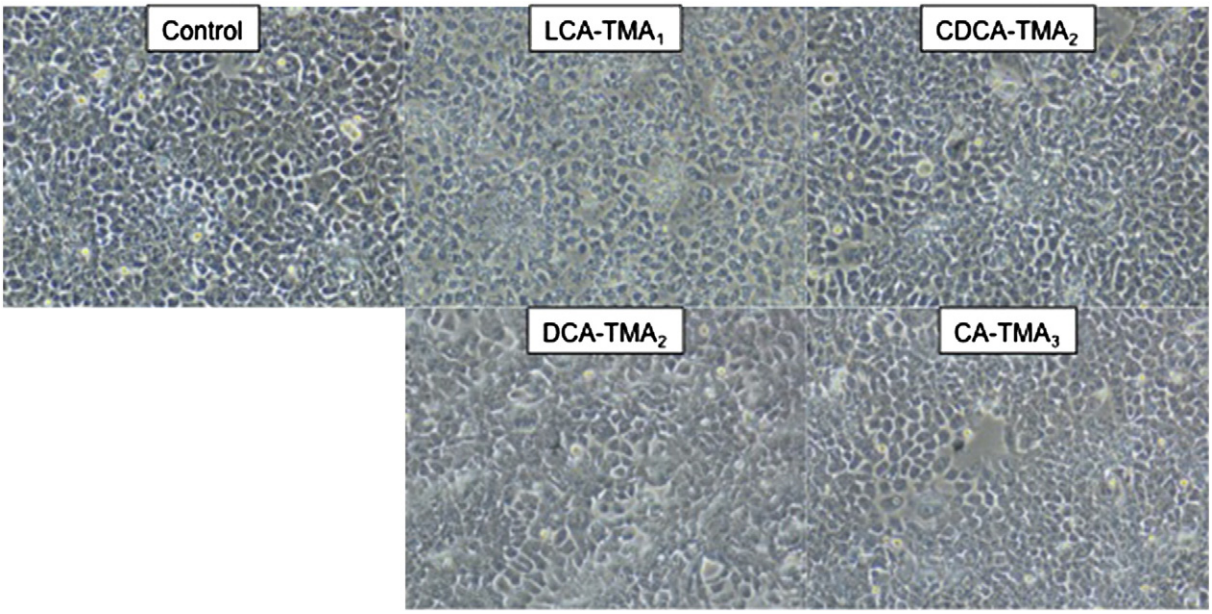

Fig. 4. Light microscopy images of HCT-116 cells treated with 50 μM of facial amphiphiles LCA-TMA_1, CDCA-TMA_2, DCA-TMA_2, and CA-TMA_3 for 48 h indicating the maximum apoptosis upon treatment with LCA-TMA_1.

cells to undergo apoptosis, whereas treatment of HCT-116 cells with CDCA-TMA_2, DCA-TMA_2 and CA-TMA_3 caused only 5% apoptosis (Fig. 6). Treatment of DLD-1 cells with 100 μM of facial amphiphiles (Fig. 7) also caused cells to undergo late apoptosis. We observed ~64% cells in late apoptosis on treatment with LCA-TMA_1 whereas other amphiphiles caused only 2–4% apoptosis. Therefore light microscopy and Annexin-FITC studies confirmed the highest apoptotic effect of LCA-TMA_1 as compared to other amphiphiles.

3.4. Facial amphiphile-membrane interactions

Interactions of facial amphiphiles with cell membranes involve complex events of adsorption, penetration, and translocation [28]. These complex events require two steps: 1) Electrostatic interactions between cationic amphiphiles and cell membranes causing dehydration, 2) Hydrophobic interactions of amphiphiles with hydrophobic part of membranes causing perturbations [29]. Therefore to explore the differential activity of facial amphiphiles, we studied the changes in membrane hydration and membrane perturbations [30,31] upon interactions of these amphiphiles with model DPPC membranes [32,33].

To explore the alterations in membrane hydration, we studied the changes in generalized polarization of Prodan doped in DPPC membranes upon incubation with facial amphiphiles. Generalized polarization of Prodan decreases on increase in hydration and increases in dehydrated environment. Incubation with 10 mol% of facial amphiphiles resulted in dehydration on membrane surface after 12 h of incubation with no further enhancement in dehydration even after prolonged incubation

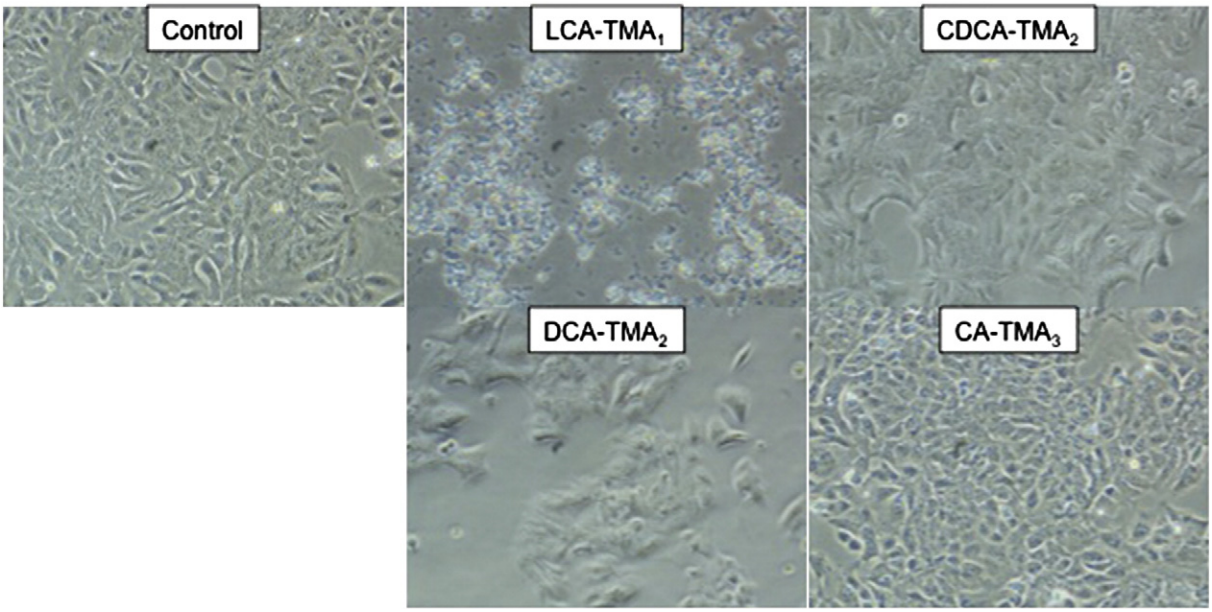

Fig. 5. Light microscopy images of DLD-1 cells treated with 100 μM of facial amphiphiles LCA-TMA_1, CDCA-TMA_2, DCA-TMA_2, and CA-TMA_3 for 48 h indicating the maximum apoptotic bodies upon treatment with LCA-TMA_1.

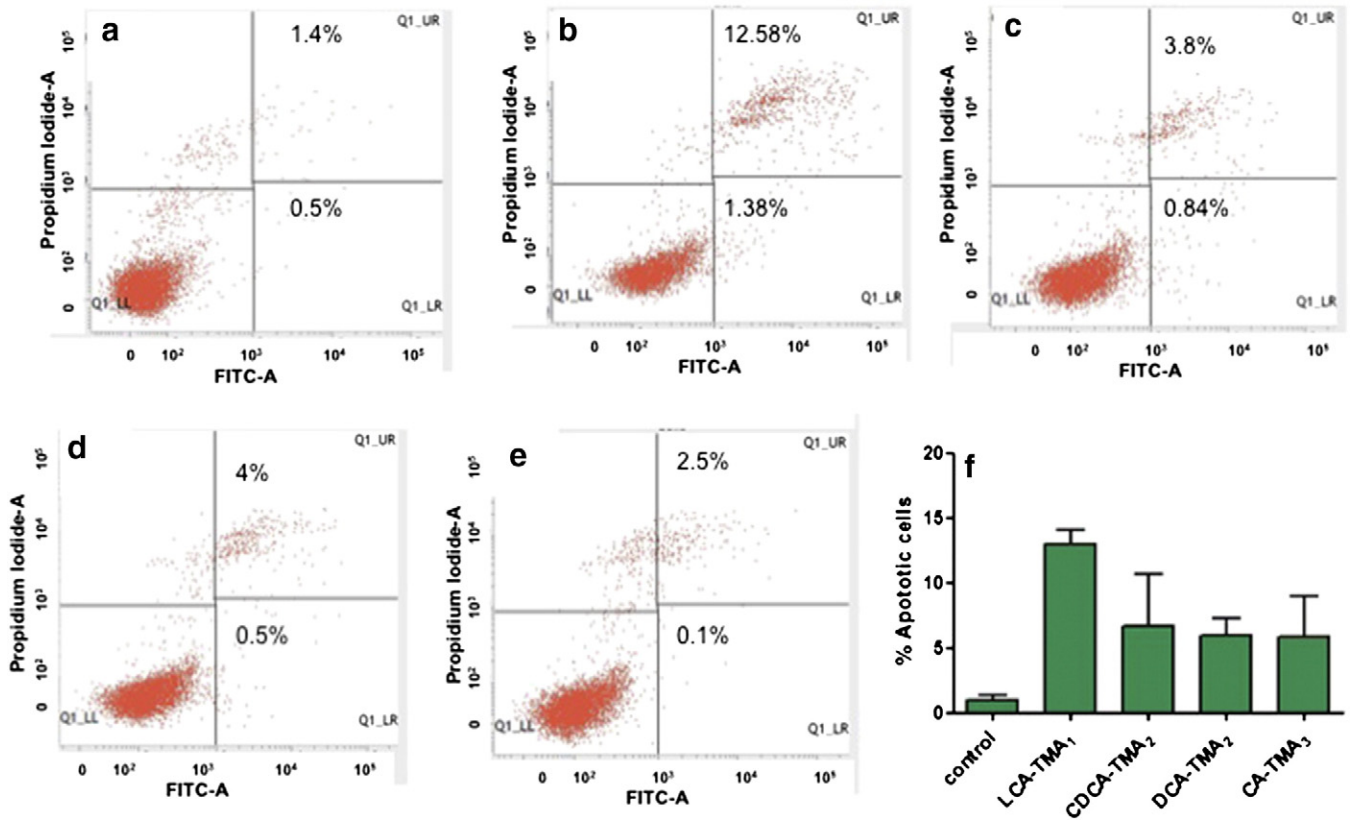

Fig. 6. Annexin-FITC based apoptosis assay of HCT-116 cells upon treatment with 50 μM of facial amphiphiles, a) Control, b) LCA-TMA_1, c) CDCA-TMA_2, d) DCA-TMA_2, and e) CA-TMA_3 for 48 h indicating the maximum apoptposis upon treatment with LCA-TMA_1 amphiphile f).

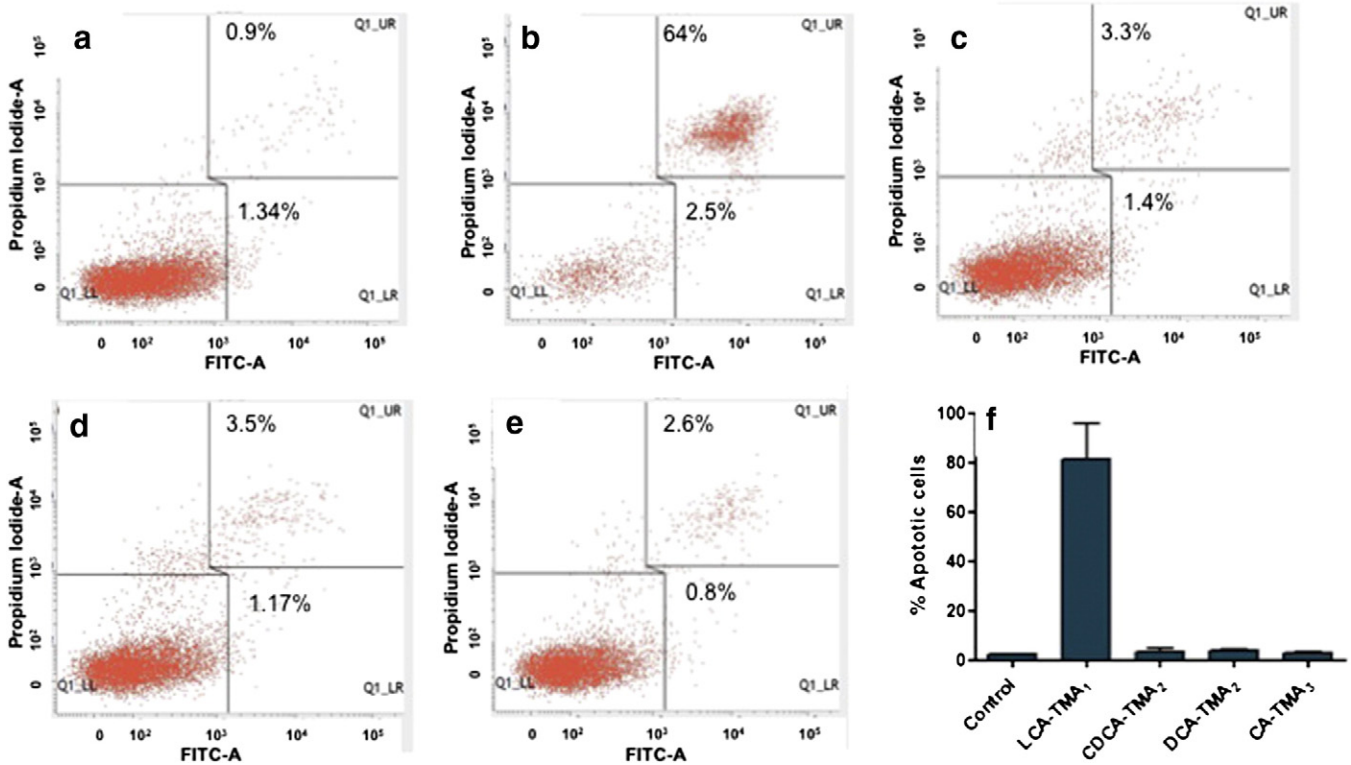

Fig. 7. Annexin-FITC based apoptosis assay of DLD-1 cells upon treatment with 100 μM of facial amphiphiles, a) Control, b) LCA-TMA_1, c) CDCA-TMA_2, d) DCA-TMA_2, and e) CA-TMA_3 for 48 h indicating the maximum apoptposis upon treatment with LCA-TMA_1 amphiphile f).

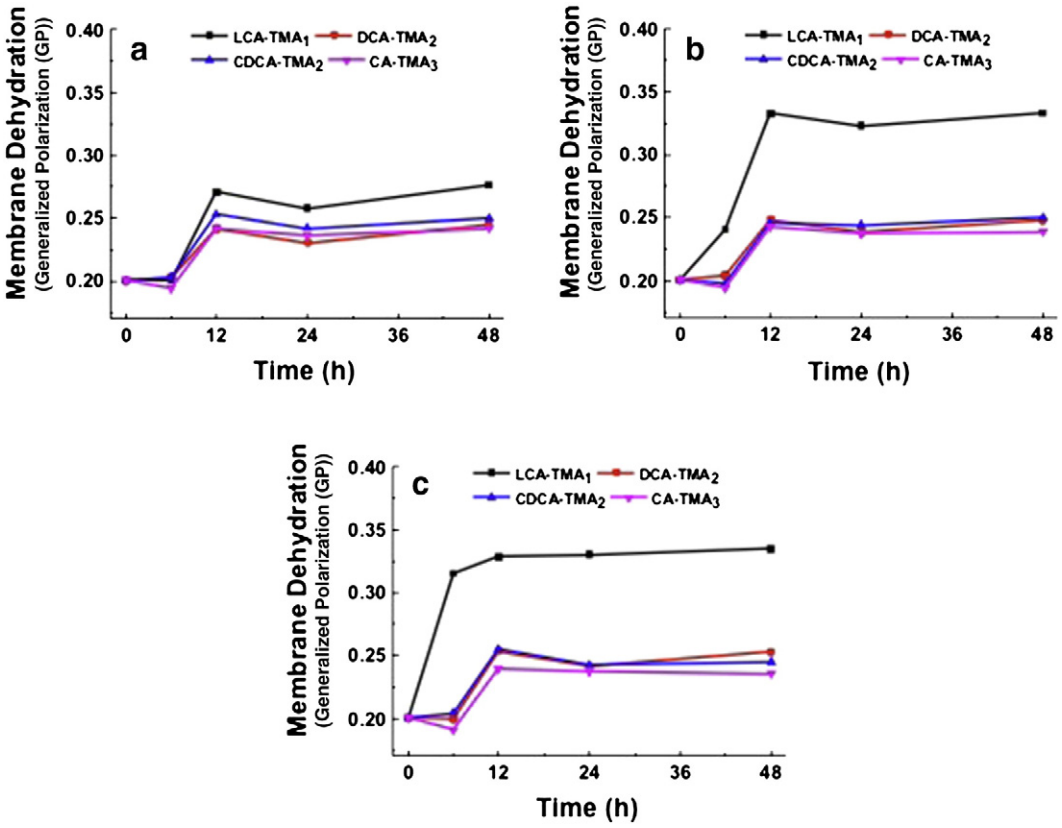

Fig. 8. Time dependent changes in generalized polarization or membrane dehydration on incubation of Prodan-doped DPPC liposomes with 10 (a), 20 (b), and 30 (c) mol percentages of facial amphiphiles LCA-TMA_1, CDCA-TMA_2, DCA-TMA_2, and CA-TMA_3 at 37 °C indicating the maximum dehydration on incubation with LCA-TMA_1 amphiphile.

for 24 h and 48 h, indicating that maximum interactions occur after 12 h. Upon increasing the concentration to 20 or 30 mol%, LCA-TMA_1 amphiphile induced dehydration of DPPC membranes after 6 h (Fig. 8b, c), whereas there was no dehydration after 6 h upon incubation with CDCA-TMA_2, DCA-TMA_2 and CA-TMA_3 with DPPC membranes. The singly charged LCA-TMA_1 showed three-fold enhancement in dehydration as

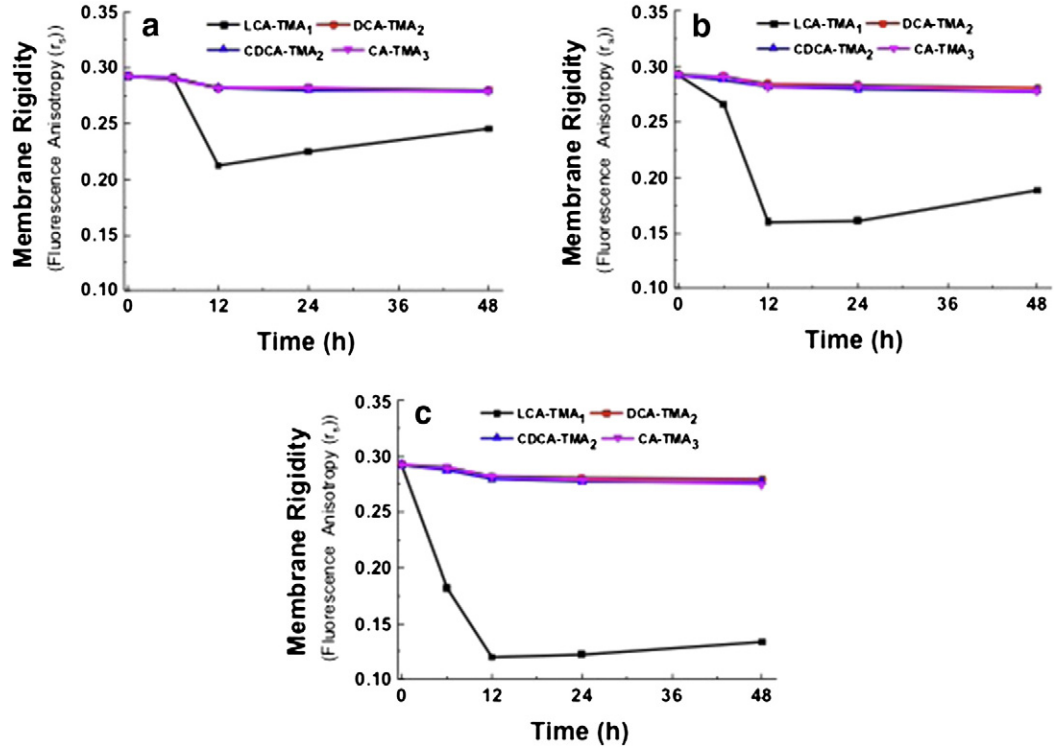

Fig. 9. Time dependent changes in fluorescence anisotropy or membrane rigidity (fluidity) on incubation of DPPC liposomes with 10 (a), 20 (b), and 30 (c) mol percentages of facial amphiphiles LCA-TMA_1, CDCA-TMA_2, DCA-TMA_2, and CA-TMA_3 at 37 °C indicating the maximum fluidity of DPPC membranes on incubation with LCA-TMA_1 amphiphile.

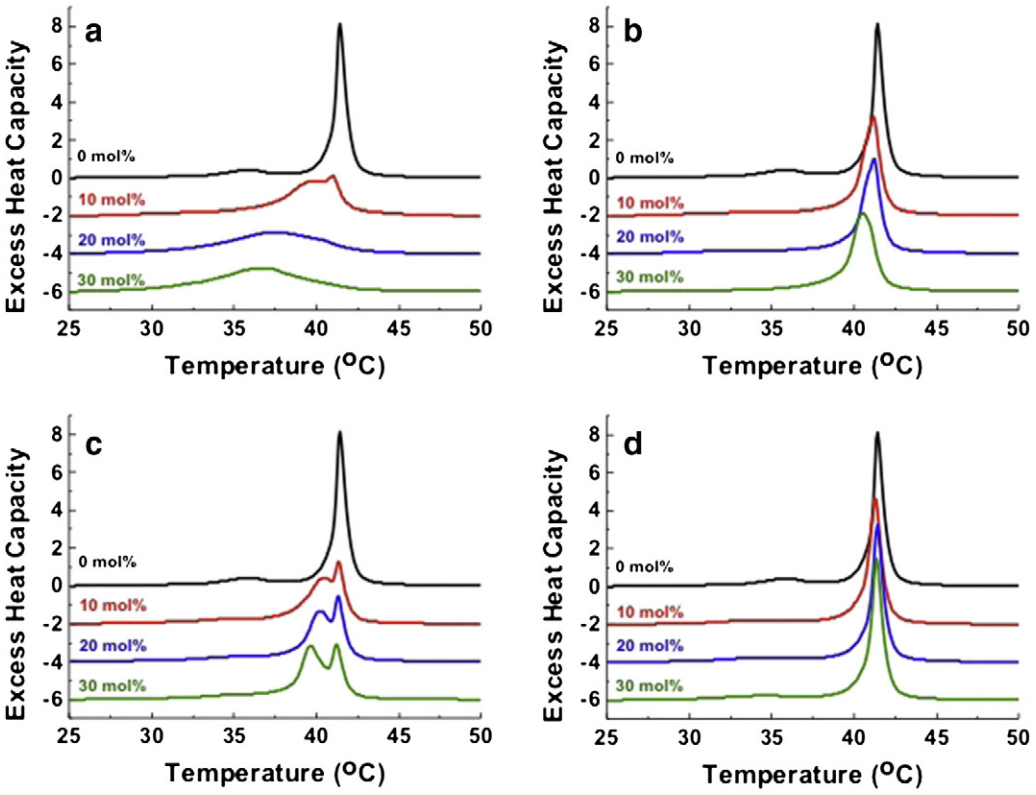

Fig. 10. Differential thermal scans of DPPC liposomes on incubation with 10, 20, 30 mol percentages of various facial amphiphiles a) LCA-TMA_1, b) CDCA-TMA_2, c) DCA-TMA_2, d) CA-TMA_3 at 37 °C for 24 h.

compared to other amphiphiles indicating its strong electrostatic interactions with DPPC membranes as compared to other multiple charged amphiphiles.

We then studied changes in membrane perturbations of DPH-doped DPPC membranes on incubation with amphiphiles at 37 °C (Fig. 9). Incubation of 10 mol% of LCA-TMA_1 (Fig. 9a) showed increased membrane perturbations of DPPC membranes after 12 h, whereas multiple charged amphiphiles CDCA-TMA_2, DCA-TMA_2 and CA-TMA_3 did not show membrane perturbations. We demonstrate 2- and 3-fold increase in membrane perturbations upon incubation with 20% and 30% of LCA-TMA_1 amphiphile after 12 h, respectively (Fig. 9b/c). However, we observed slight decrease in fluidity after 24 h and 48 h of incubation due to minor adjustments of LCA-TMA_1 in hydrophobic environment of DPPC membranes. Increase in membrane fluidity on incubation of LCA-TMA_1 indicates strong penetration of amphiphile in DPPC membranes. We observed that penetration of LCA-TMA_1 in membranes strongly depends on concentration of amphiphile and time of incubation with membranes. There is no change in membrane fluidity of DPPC membranes on incubation with multiple charged facial amphiphiles CDCA-TMA_2, DCA-TMA_2, and CA-TMA_3 at different concentrations even up to 48 h (Fig. 9). Therefore, DPH-based studies showed that introduction of multiple charges on bile acid did not enhance membrane perturbations by theses multiple charged bile acid based facial amphiphiles.

To explore the membrane perturbations further, we studied the interactions of amphiphiles with DPPC membranes by calorimetry studies. DPPC membranes were first incubated with different concentrations of facial amphiphiles for 24 h at 37 °C to mimic *in vitro* cell culture conditions. We then performed differential scanning calorimetry studies on DPPC membranes [34]. LCA-TMA_1 on 10 mol% of its incubation with DPPC liposomes causes broadening of phase transition of DPPC membranes (Fig. 10a). Phase transition of DPPC membranes gets abolished on incubation with 20 and 30 mol% of LCA-TMA_1 indicating that LCA-TMA_1 amphiphile perturbs DPPC membranes. CDCA-TMA_2 amphiphile did not perturb DPPC membranes packing upon incubation with DPPC membranes as observed in LCA-TMA_1 (Fig. 10b). We observed sharp and broad transitions upon incubation with DCA-TMA_2 with DPPC membranes indicating phase separation. CA-TMA_3 possessing three head groups did not change phase behavior of liposomes on incubation with DPPC membranes (Fig. 10d), indicating that CA-TMA_3 does not perturb the DPPC membranes. Thus, the order of perturbation with DPPC membrane for these amphiphiles is LCA-TMA_1 > DCA-TMA_2 > CDCA-TMA_2 > CA-TMA_3.

Differential scanning thermograms of DPPC membranes shows two phase transitions: a pre-transition at 35 °C arising from conversion of lamellar to rippled gel phase, and the second main transition of rippled gel phase to lamellar liquid-crystalline phase. Pre-transition of DPPC membranes get diminished upon incubation with facial amphiphiles with DPPC membranes. Incubation of LCA-TMA_1 amphiphile with DPPC membranes decreases phase transition (T_m) of liposomes from

Table 1
Thermodynamic characterization of phase transition exhibited by DPPC liposomes on incubation with 10%, 20%, 30% mol percentages of various facial amphiphiles LCA-TMA_1, CDCA-TMA_2, DCA-TMA_2, CA-TMA_3 at 37 °C for 24 h as determined from differential scanning calorimetry.

Amphiphile	Doping (%)	T_m (°C)	ΔH_c (Kcal/mol)	FWHM	C_p^{max}	ΔH_{vH}	CU
DPPC	100%	41.41	10.84	0.682	9.44	999.25	92.18
LCA-TMA_1	10 mol%	41.06	9.84	3.00	2.33	226.85	23.05
LCA-TMA_1	20 mol%	37.75	8.71	5.69	1.27	117.10	13.44
LCA-TMA_1	30 mol%	36.96	8.9	5.42	1.39	122.30	13.74
CDCA-TMA_2	10 mol%	41.21	10.88	1.08	5.99	630.45	57.97
CDCA-TMA_2	20 mol%	41.16	10.35	1.07	5.76	636.45	61.49
CDCA-TMA_2	30 mol%	40.39	9.93	1.47	4.75	461.00	46.42
DCA-TMA_2	10 mol%	41.33	9.65	1.63	3.75	418.24	43.34
DCA-TMA_2	20 mol%	41.31	9.77	1.59	3.88	428.71	43.88
DCA-TMA_2	30 mol%	41.26	9.6	1.90	3.31	358.65	37.35
CA-TMA_3	10 mol%	41.26	10.37	1.08	5.73	630.96	60.84
CA-TMA_3	20 mol%	41.34	10.71	0.76	8.33	897.08	83.76
CA-TMA_3	30 mol%	41.29	10.85	0.76	8.67	896.80	82.65

41 °C to 36 °C, whereas incubation of CDCA-TMA_2, DCA-TMA_2, and CA-TMA_3 does not change T_m (Table 1). Enthalpy of transition of membranes decreases only on interactions of LCA-TMA_1 with DPPC liposomes. Co-operativity unit (CU) of liposome–amphiphile interactions strongly depends on perturbation of membranes. CU decreases with increase in concentration of LCA-TMA_1 incubation as this amphiphile causes maximum perturbations in membranes. There is minor change in co-operativity of DPPC liposomes on incubation with CA-TMA_3, as it does not cause any perturbations due to minimal penetration with membranes. Phase transition of DPPC membranes on interactions with facial amphiphiles shows asymmetric endotherms due to incorporation of amphiphiles in membranes. This asymmetry of endotherms strongly depends on nature of amphiphile and amount of penetration of these amphiphiles in membranes. These asymmetric DSC endotherms consist of a) sharp component due to chain melting of amphiphile-poor DPPC domains, b) broad component of amphiphile-rich DPPC domains. We decomposed endotherms of these transitions into sharp and broad components as shown in Fig. 11. Phase transition temperature (T_m) and co-operativity (CU) in sharp component of transition in general decreases with increase in % of incubation (Table 2). Incubation of LCA-TMA_1 lowers

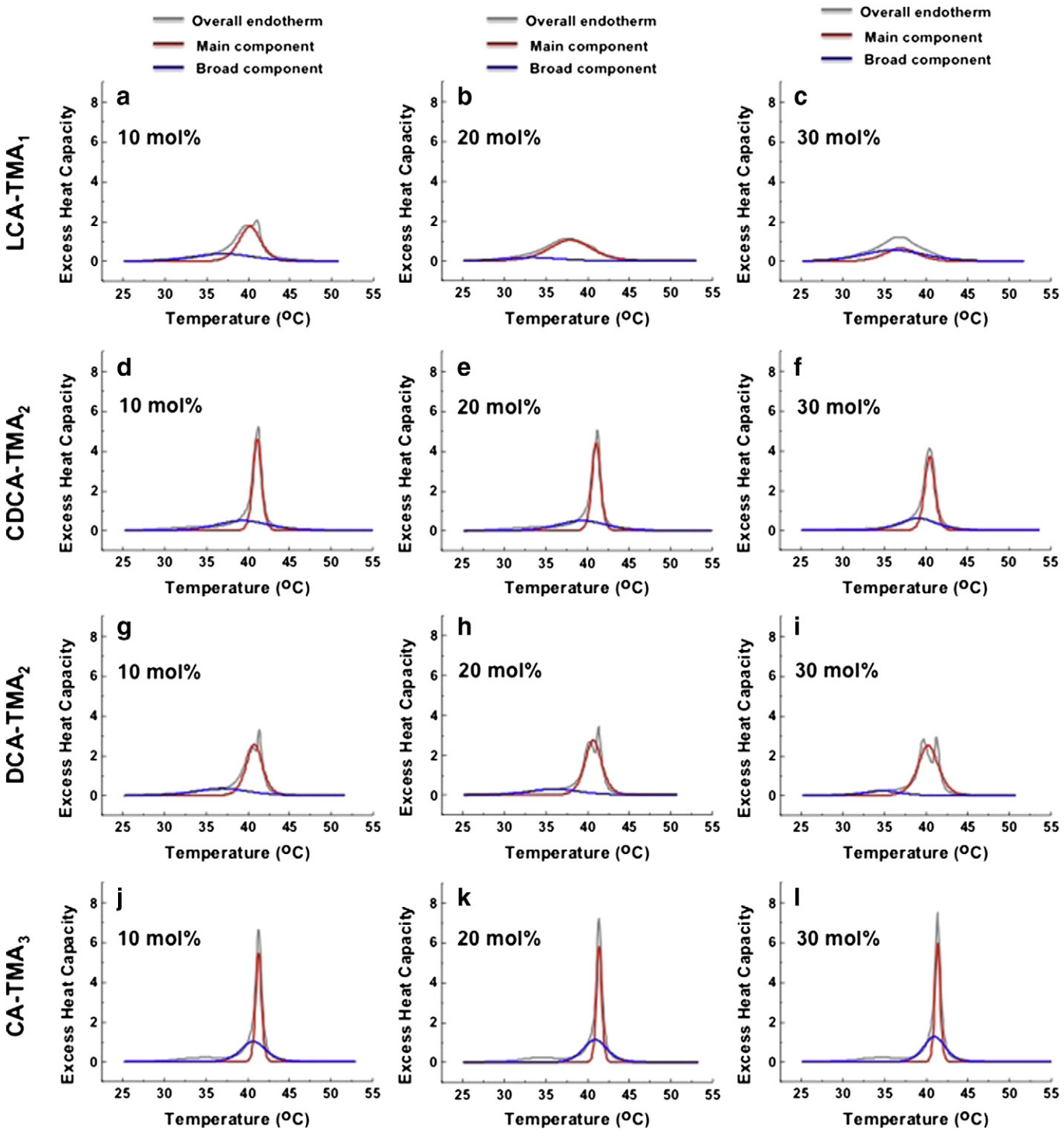

Fig. 11. Decomposed endotherms of main phase transition of DPPC liposomes on incubation with 10, 20, 30 mol percentages of various facial amphiphiles LCA-TMA_1 (a, b, c); CDCA-TMA_2 (d, e, f); DCA-TMA_2 (g, h, i); and CA-TMA_3 (j, k, l) at 37 °C for 24 h.

Table 2
Thermodynamic characterization of sharp component of phase transition exhibited by DPPC liposomes on incubation with 10%, 20%, 30% mol percentages of facial amphiphiles LCA-TMA_1, CDCA-TMA_2, DCA-TMA_2, CA-TMA_3 at 37 °C for 24 h as determined from differential scanning calorimetry.

Amphiphile	Doping (%)	T_m (°C)	ΔH_c (Kcal/mol)	FWHM	C_p^{max}	ΔH_{vH}	CU
LCA-TMA_1	10 mol%	40.18	6.03	2.63	2.035	257.12	42.57
LCA-TMA_1	20 mol%	37.92	7.15	5.15	1.22	129.52	18.11
LCA-TMA_1	30 mol%	37.00	3.42	3.86	0.76	171.78	50.22
CDCA-TMA_2	10 mol%	41.09	6.11	0.97	5.39	687.44	114.14
CDCA-TMA_2	20 mol%	41.06	5.39	0.95	5.17	713.38	132.35
CDCA-TMA_2	30 mol%	40.47	5.85	1.13	4.34	600.01	102.56
DCA-TMA_2	10 mol%	40.75	6.63	1.88	3.00	361.29	54.49
DCA-TMA_2	20 mol%	40.66	7.36	2.00	3.20	339.42	46.11
DCA-TMA_2	30 mol%	40.23	8.20	2.50	2.95	270.792	33.01
CA-TMA_3	10 mol%	41.28	4.93	0.84	5.32	811.34	164.57
CA-TMA_3	20 mol%	41.35	4.76	0.56	6.84	1200.40	252.18
CA-TMA_3	30 mol%	41.34	4.84	0.56	6.99	1217.47	251.54

CU and T_m of DPPC membranes, whereas increase in CU and no change in T_m was observed for CA-TMA_3. Increase in CU for CA-TMA_3 may be due to weak surface interactions of these amphiphiles with phospholipids. In broad component of transition, (Table 3) enthalpy of transition decreases and co-operativity increases with increase in % of incubation that may be due to incorporation of more amphiphiles in amphiphile rich domains leading to more hydrophobic interactions among bile acid amphiphiles.

These results indicate that balance of electrostatic and hydrophobic interactions of amphiphiles with cellular membranes is responsible for activities of these amphiphiles. Multiple charged CA-TMA_3 does not show electrostatic interactions with DPPC membranes due to its high hydration. Highly charged surface and low hydrophobicity does not allow CA-TMA_3 molecules to perturb the DPPC membranes making them less active. Single charged, Lithocholic acid based LCA-TMA_1 amphiphile showed strong electrostatic interactions with phospholipids causing maximum dehydration. Hydrophobicity of LCA-TMA_1 allows this amphiphile to perturb DPPC membranes causing maximum perturbations making it most active.

CDCA-TMA_2 and DCA-TMA_2 showed intermediate cytotoxic behavior, where DCA-TMA_2 is more potent than CDCA-TMA_2 in HCT-116 and DLD-1 cell lines, although both amphiphiles possess two trimethyl ammonium head groups. DCA-TMA_2 amphiphile possess ammonium head groups at 3′- and 12′-carbon positions, whereas CDCA-TMA_2 have ammonium head groups at 3′- and 7′-carbon positions. Small change in T_m indicates lower miscibility of CDCA-TMA_2 with DPPC membranes and therefore, we observe marginal cytotoxicity. In contrast, DCA-TMA_2 shows more broadened and lowered T_m. Thus, DCA-TMA_2 amphiphile has a better tendency to penetrate into DPPC membranes causing more perturbations as compared to CDCA-TMA_2. Therefore, the differential interactions of CDCA-TMA_2 and DCA-TMA_2 with DPPC membranes are due to different positioning of trimethyl ammonium head groups in these two amphiphiles, and cytotoxic activities showed that DCA-TMA_2 amphiphile is more active as compared to CDCA-TMA_2. Thus, these studies showed that interactions of facial amphiphiles with DPPC membranes strongly depend on hydrophobicity and charge distribution on these amphiphiles. Charge is required for favorable electrostatic interactions, and hydrophobicity facilitates membrane perturbations in these amphiphiles. These interactions account for differential adsorption, perturbation and translocation behavior with cell membrane and thereby account for distinctive cytotoxic activities in these amphiphiles.

Table 3
Thermodynamic characterization of broad component of phase transition exhibited by DPPC liposomes on incubation with 10%, 20%, 30% mol percentages of facial amphiphiles LCA-TMA_1, CDCA-TMA_2, DCA-TMA_2, CA-TMA_3 at 37 °C for 24 h as determined from differential scanning calorimetry.

Amphiphile	Doping (%)	T_m (°C)	ΔH_c (Kcal/mol)	FWHM	C_p^{max}	ΔH_{vH}	CU
LCA-TMA_1	10 mol%	37.03	4.61	6.78	0.43	97.81	21.21
LCA-TMA_1	20 mol%	33.39	3.71	5.02	0.18	129.03	34.77
LCA-TMA_1	30 mol%	36.16	1.61	6.92	0.63	95.30	59.19
CDCA-TMA_2	10 mol%	39.39	4.24	6.12	0.58	110.02	25.94
CDCA-TMA_2	20 mol%	39.29	3.97	5.66	0.59	118.89	29.94
CDCA-TMA_2	30 mol%	39.09	3.68	4.47	0.71	150.34	40.85
DCA-TMA_2	10 mol%	36.96	3.01	6.02	0.41	110.11	36.58
DCA-TMA_2	20 mol%	36.02	2.42	5.67	0.34	116.20	48.02
DCA-TMA_2	30 mol%	34.73	1.42	3.96	0.27	165.00	116.19
CA-TMA_3	10 mol%	40.67	4.1	3.68	1.00	184.47	44.99
CA-TMA_3	20 mol%	40.88	4.36	2.86	1.34	237.68	54.51
CA-TMA_3	30 mol%	40.95	4.37	2.55	1.49	266.70	61.03

4. Conclusions

We have synthesized four bile acid based facial amphiphiles possessing trimethyl ammonium head groups. Activities of these amphiphiles against colon cancer cell lines showed a structure-activity relationship in order of LCA-TMA_1 > DCA-TMA_2 > CDCA-TMA_2 > CA-TMA_3. Light microscopy and Annexin-FITC studies showed that these amphiphiles could trigger late apoptosis. We demonstrate that the interactions of these amphiphiles with model membrane systems showed that their activities strongly contingent upon the charge, hydration, and hydrophobicity. LCA-TMA_1 amphiphile is most potent as it shows strong electrostatic interactions with DPPC membranes. In addition, high hydrophobicity of LCA-TMA_1 caused maximum perturbations of membranes leading to effective translocation. The highly hydrated and multiple charged DCA-TMA_2, CDCA-TMA_2, CA-TMA_3 does not show strong interactions with membranes. Thus, these amphiphiles do not perturb the cell membranes rendering them less active. These results establish a new class of facial amphiphiles as cytotoxic agents against colon cancer for potential therapeutic significance.

Acknowledgements

We thank Prof. Dinakar Salunke for his support and encouragement, RCB for intramural funding, and Department of Biotechnology, Department of Science and Technology for funding. A.B. thanks Department of Science and Technology for Ramanujan Fellowship. SK thanks RCB, and AS thanks DBT for research fellowships. We thank Vishakha Chaudhary for helping in recording Mass spectra, Vijay Kumar Jha for helping in DSC experiments, and AIRF, JNU for recording NMR spectra. We thank Dr. Bishwajit Paul for reading and editing the manuscript, and his comments.

References

[1] A.F. Hofmann, The continuing importance of bile acids in liver and intestinal disease, Arch. Intern. Med. 159 (1999) 2647–2658.
[2] S. Mukhopadhyay, U. Maitra, Chemistry and biology of bile acids: a review, Curr. Sci. 87 (2004) 1666–1683.
[3] A.A. Powell, J.M. Larue, A.K. Batta, J.D. Martinez, Bile acid hydrophibicty is correlated with induction of apoptosis and/or growth arrest in HCT116 cells, Biochem. J. 356 (2001) 481–486.
[4] J.Y.L. Chiang, Bile acid regulation of hepatic physiology III. Bile acids as nuclear receptors, Am. J. Physiol. Gastrointest. Liver Physiol. 284 (2003) G349–G356.
[5] S.R. McGarr, J.M. Ridlon, P.B. Hylemon, Diet, anaerobicbacterial metabolism, and colon cancer: a review of the literature, J. Clin. Gastroenterol. 39 (2005) 98–109.
[6] J.R. Pearson, C.I. Gill, I.R. Rowland, Diet, fecal water, and colon cancer development of a biomarker, Nutr. Rev. 67 (2009) 509–526.
[7] H. Zeng, J.H. Botnen, M. Briske-Anderson, Deoxycholic acid and selenium metabolite methylselenol exert common and distinct effects on cell cycle, apoptosis, and MAP kinase pathway in HCT116 human colon cancer cells, Nutr. Cancer 62 (2010) 85–92.
[8] S.A. Shah, E. Looby, Y. Volkov, A. Long, D. Kelleher, Ursodeoxycholic acid inhibits translocation of protein kinase C in human colonic cancer cell lines, Eur. J. Cancer 41 (2005) 2160–2169.
[9] A. Zimber, C. Gespach, Bile acids and derivatives, their nuclear receptors FXR, PXR and ligands: Role in health and disease and their therapeutic potential, Anticancer Agents Med. Chem. 8 (2008) 540–563.
[10] L. Mi, S. Devarakonda, J.M. Harp, Q. Han, R. Pellicciari, T.M. Wilson, S. Khorasanizadeh, F. Rastinejad, Structural basis for bile acid binding and activation of the nuclear receptor FXR, Mol. Cell 11 (2003) 1093–1100.

[11] C. Degirolamo, S. Modica, G. Palasciano, A. Moschetta, Bile acids and colon cancer: solving the puzzle with nuclear receptors, Trends Mol. Med. 17 (2011) 564–572.
[12] N.D. Kim, E.O. Im, Y.H. Choi, Y.H. Yoo, Synthetic bile acids: novel mediators of apoptosis, J. Biochem. Mol. Biol. 35 (2002) 134–141.
[13] E. Ima, S. Choia, H. Suhb, Y. Hyun, C.Y.H. Yood, N.D. Kim, Synthetic bile acid derivatives induce apoptosis through a c-Jun N-terminal kinase and NF-kB-dependent processing human cervical carcinoma cells, Cancer Lett. 229 (2005) 49–57.
[14] F.M. Nagengast, M.J.A.L. Grubben, I.P. Van Muster, Role of bile acids in colorectal carcinogenesis, Eur. J. Cancer 31A (1995) 1067–1070.
[15] R. Sharma, F. Majer, V.K. Peta, J. Wang, R. Keaveney, D. Kelleher, A. Long, J.F. Gilmer, Bile acid toxicity structure–activity relationships: correlations between cell viability and lipophilicity in a panel of new and known bile acids using an oesophageal cell line (HET-1A), Bioorg. Med. Chem. 18 (2010) 6886–6895.
[16] L.E. Kihel, M. Clement, M. Bazin, G. Descamps, M. Khalid, S. Rault, New lithocholic and chenodeoxycholic piperazinylcarboxamides with antiproliferative and pro-apoptotic effects on human cancer cell lines, Bioorg. Med. Chem. 16 (2008) 8737–8744.
[17] E. Im, Y.H. Choi, K. Paik, H. Suh, Y. Jin, K. Kim, Y.H. Yoo, N.D. Kim, Novel bile acid derivatives induce apoptosis via a p53-independent pathway in human breast carcinoma cells, Cancer Lett. 163 (2001) 83–93.
[18] B.W. Katona, S. Anant, D.F. Covey, W.F. Stenson, Characterization of enantiomeric bile acid-induced apoptosis in colon cancer cell lines, J. Biol. Chem. 284 (2009) 3354–3364.
[19] A. Bajaj, P. Kondaiah, S. Bhattacharya, Synthesis and gene transfection properties of PEI cholesterol based lipopolymers, Bioconjug. Chem. 19 (2008) 1640–1651.
[20] S.W. Fesik, Promoting apoptosis as a strategy for cancer drug discovery, Nat. Rev. Cancer 5 (2005) 876–885.
[21] S. Bhattacharya, A. Bajaj, Membrane-forming properties of pseudoglyceryl backbone based gemini lipids possessing oxyethylene spacers, J. Phys. Chem. B 111 (2007) 2463–2472.
[22] T. Parasassi, E.K. Krasnowska, L. Bagatolli, E. Gratton, Laurdan and prodan as polarity-sensitive fluorescent membrane probes, J. Fluoresc. 8 (1998) 365–373.
[23] V. Sreekanth, A. Bajaj, Fluorescence (fluidity/hydration) and calorimetric studies of interactions of bile acid–drug conjugates with model membranes, J. Phys. Chem. B 117 (2013) 2123–2133.
[24] S. Bhattacharya, A. Bajaj, Fluorescence and thermotropic studies of the interactions of PEI-cholesterol based PEI-chol lipopolymers with dipalmitoyl phosphatidylcholine membranes, Biochim. Biophys. Acta 1778 (2008) 2225–2233.
[25] J.M. Sturtevant, A scanning calorimetric study of small molecule–lipid bilayer mixtures, Proc. Natl. Acad. Sci. U. S. A. 79 (1982) 3963–3967.
[26] H.J. Hinz, J.M. Sturtevant, Calorimetric studies of dilute aqueous suspensions of bilayers formed from synthetic L-α-lecithins, J. Biol. Chem. 247 (1972) 6071–6075.
[27] T.P.W. McMullen, R.N. McElhaney, New aspects of the interaction of cholesterol with dipalmitoylphosphatidylcholine bilayers as revealed by high-sensitivity differential scanning calorimetry, Biochim. Biophys. Acta 1234 (1995) 90–98.
[28] C. Peetla, A. Stine, V. Labhasetwar, Biophysical interactions with model lipid membranes: applications in drug discovery and drug delivery, Mol. Pharm. 6 (2009) 1264–1276.
[29] K. Kawano, E. Onose, Y. Hattori, Y. Maitani, Higher liposomal membrane fluidity enhances the in vitro antitumor activity of folate-targeted liposomal mitoxantrone, Mol. Pharm. 6 (2009) 98–104.
[30] B. Gzyl-Malcher, M. Filek, G. Brezesinski, Mixed DPPC/DPTAP monolayers at the air/water interface: influence of Indolilo-3-acetic Acid and Selenate Ions on the monolayer morphology, Langmuir 27 (2011) 10886–10893.
[31] F. Castelli, M. Grazia Sarpietro, M. Ceruti, F. Rocco, L. Cattel, Characterization of lipophilic gemcitabine prodrug-liposomal membrane interaction by differential scanning calorimetry, Mol. Pharm. 3 (2006) 738–746.
[32] A. Grancelli, A. Morros, M.E. Cabanas, O. Domenech, S. Merino, J.L. Vazquez, M.T. Montero, M. Vinas, J. Hernandez-Borrell, Interaction of 6-fluoroquinolones with dipalmitoylphosphatidylcholine monolayers and liposomes, Langmuir 18 (2002) 9177–9182.
[33] M. Lucio, F. Bringezu, S. Reis, J.F.C. Lima, G. Brezesinski, Binding of non-steroidal anti-inflammatory drugs to DPPC: structure and thermodynamic actions, Langmuir 24 (2008) 4132–4139.
[34] J.K. Seydel, E.A. Coats, H.P. Cordes, M. Wiese, Drug membrane interaction and the importance for drug transport, distribution, accumulation, efficacy and resistance, Arch. Pharm. (Weinheim) 327 (1994) 601–610.